THE JOURNAL OF PHYSICAL CHEMISTRY B

Article

pubs.acs.org/JPCB

Open Access on 08/15/2015

Characterizing Solution Surface Loop Conformational Flexibility of the GM2 Activator Protein

Jeffery D. Carter,[†,⊥] Jordan D. Mathias,[†,#] Edwin F. Gomez,[‡] Yong Ran,[†,○] Fang Xu,[§] Luis Galiano,[†,▽] Nguyen Q. Tran,[‡] Peter W. D'Amore,[†,&] Christine S. Wright,[∥] Dhruva K. Chakravorty,[‡] and Gail E. Fanucci*[,†]

[†]Department of Chemistry, University of Florida, P.O. Box 117200, Gainesville, Florida 32611-7200, United States

[‡]Department of Chemistry, University of New Orleans, 2000 Lakeshore Drive, New Orleans, Louisiana 70148, United States

[§]Department of Pathology, University of Virginia, P.O. Box 800904, Charlottesville, Virginia 22906, United States

[∥]Department of Pharmacology, University of Virginia, Charlottesville, Virginia 22908, United States

Supporting Information

ABSTRACT: GM2AP has a β-cup topology with numerous X-ray structures showing multiple conformations for some of the surface loops, revealing conformational flexibility that may be related to function, where function is defined as either membrane binding associated with ligand binding and extraction or interaction with other proteins. Here, site-directed spin labeling (SDSL) electron paramagnetic resonance (EPR) spectroscopy and molecular dynamic (MD) simulations are used to characterize the mobility and conformational flexibility of various structural regions of GM2AP. A series of 10 single cysteine amino acid substitutions were generated, and the constructs were chemically modified with the methanethiosulfonate spin label. Continuous wave (CW) EPR line shapes were obtained and subsequently simulated using the microscopic order macroscopic disorder (MOMD) program. Line shapes for sites that have multiple conformations in the X-ray structures required two spectral components, whereas spectra of the remaining sites were adequately fit with single-component parameters. For spin labeled sites L126C and I66C, spectra were acquired as a function of temperature, and simulations provided for the determination of thermodynamic parameters associated with conformational change. Binding to GM2 ligand did not alter the conformational flexibility of the loops, as evaluated by EPR and NMR spectroscopies. These results confirm that the conformational flexibility observed in the surface loops of GM2AP crystals is present in solution and that the exchange is slow on the EPR time scale (>ns). Furthermore, MD simulation results are presented and agree well with the conformational heterogeneity revealed by SDSL.

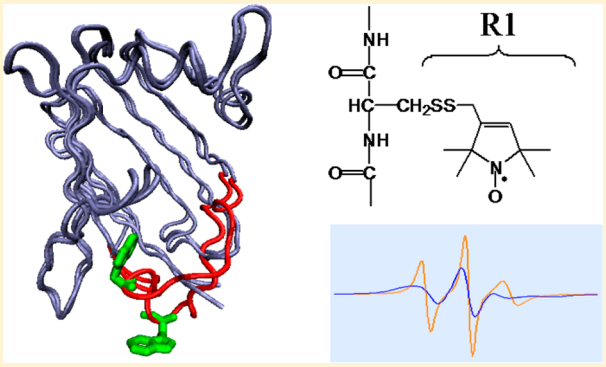

INTRODUCTION

Glycosphingolipid (GSL) catabolism occurs in lysosomal compartments within the cell.[1−3] GSLs are endocytosed, trafficked, and sorted through early and late endosomal compartments on the way to the lysosome, where specific enzymes sequentially cleave sugar groups, eventually producing ceramide, which is finally deacylated to sphingosine.[4] More than 10 different enzymes and five accessory proteins are involved in this important process. One of those accessory proteins, the GM2 activator protein (GM2AP), is essential for stimulating the catabolism of neuronal gangliosides by extracting ganglioside GM2 from intralysosomal vesicular membranes.[5] The resulting GM2AP−GM2 complex interacts with β-hexosaminidase A (Hex A) for hydrolysis of the terminal sugar to yield ganglioside GM3. Activator proteins often function by binding to glycosphingolipids and forming aqueous−soluble complexes, thereby providing an aqueous−soluble enzyme access to a lipid generally confined to a hydrophobic environment.[1,2,6] Genetic mutations that alter proper function of Hex A or GM2AP can inhibit the crucial degradation pathway, thus resulting in an accumulation of GM2 causing neuronal cell death and lysosomal storage diseases such as Tay Sachs or AB variant gangliosidosis.[7]

GM2AP is a non-homologous member of the family of proteins called sphingolipid activator proteins (SAPs). The SAPs are nonenzymatic accessory proteins required for sphingolipid hydrolysis by specific hydrolases.[2,8] Four members of this family, SAPs A−D, contain the characteristic "saposin fold" that consists of four or five α-helices anchored by three disulfide bonds. The structure of GM2AP, however, consists of eight β-strands with a tertiary β-cup topology containing four structural disulfide bonds.[9−13]

Received: June 15, 2014
Revised: August 12, 2014
Published: August 15, 2014

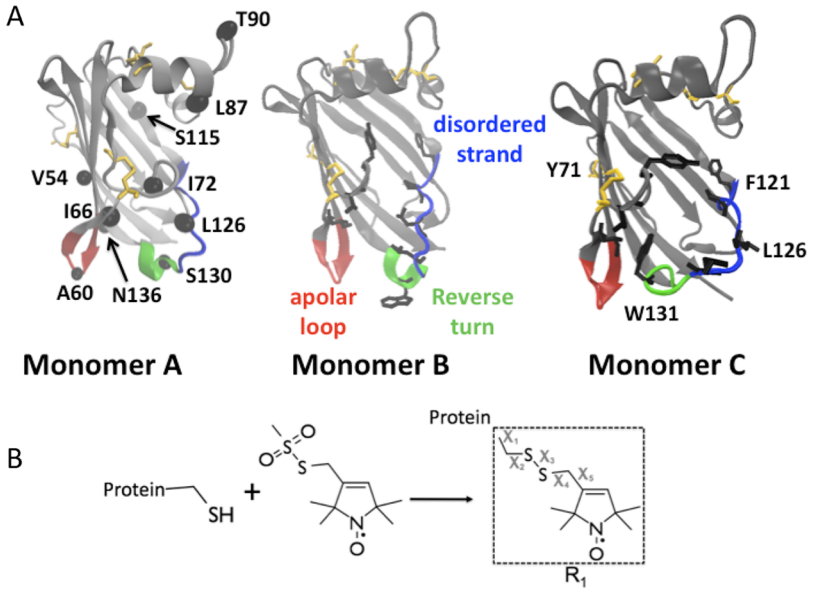

Figure 1. (A) The three unique monomers (A, B, C) of apo GM2AP (PDB ID 1G13) showing the different conformations of the loop regions at the cleft entrance. The four disulfide bonds are shown in yellow, the apolar loop (V54−W63) is shown in red, the reverse turn (S130−T133) is shown in green, and the disordered strand (V122−P129) is shown in blue. Taken together, the reverse turn and disordered strand are collectively referred to within the text as the flexible loop. Black spheres in monomer A represent the Cα positions of the reporter sites chosen for SDSL EPR experiments. Select amino acid side chains are shown in monomers B and C in stick format, demonstrating how the altered conformations in these regions modulate the size of the entrance to the lipid binding cavity.[10] Additionally, the two conformations have altered orientations of some of the amino acid side chains, including L126, L128, and W131, which alternate between pointing in toward the protein interior and extending out toward the solution. (B) SDSL labeling scheme showing the resultant R1 chemical side chain of a cysteine covalently modified with the MTSL spin label.

In addition to stimulating GM2 degradation, GM2AP has been proposed to act as a general lipid transporter because, *in vitro*, GM2AP has been shown to bind and extract GM2 from micelles, transfer glycolipids, phospholipids, and fluorescently labeled lipids between donor and acceptor vesicles,[6,14−16] bind and inhibit platelet activating factor,[12,17] and present CD1 molecules to antigens.[1,18,19] In order to carry out its function as a lipid transporter, GM2AP must partition with the lipid bilayer surface. We proposed a model of membrane partitioning based on results of sedimentation assays that showed 15% of GM2AP molecules remaining on the bilayer surface, implying that GM2AP is undergoing exchange on and off the bilayer surface.[15] From modeling of data from sedimentation assays, we concluded that GM2AP establishes exchange equilibria of a minimum of four species: GM2AP in solution, GM2AP on the bilayer surface, GM2AP−lipid complex on the bilayer surface, and GM2AP−lipid complex in solution. GM2AP−membrane interactions have also been studied by others using Langmuir monolayers, and these data suggest that GM2AP is surface associated without deep penetration into the bilayer.[20] We also showed that the orientation of GM2AP on zwitterionic bilayer surfaces is such that the mobile external loops that line the opening to the lipid binding pocket are positioned at the bilayer surface.[21]

The models of GM2AP (PDB ID 1G13) from X-ray crystallography reveal that the volume of the hydrophobic cavity is roughly 6 times larger than the volume of a ceramide moiety (500 Å^3). In addition, on the basis of X-ray structure analysis of five different crystal forms, large differences in the diameter and area of the opening to the lipid binding cavity were detected and attributed to flexibility of loop regions that decorate the rim of the cavity.[10−13] These regions (highlighted in Figure 1A) are of particular interest for this study, as their mobility may be related to function. The loops are located on opposing sides of the entrance to a prominent hydrophobic cleft whose width varies substantially among the different crystal structures. On one side of the cleft, an "apolar loop", spanning residues V54−W63, protrudes into the solution and has a relatively stable conformation in all crystal structures examined due to its involvement in crystal lattice contacts.[13] On the opposing side, a reverse turn (S130−T133) containing W131 exhibits two alternative conformations. In structures where the cleft is wide open and bound to lipid (PDB ID 1PUB), this loop is flipped out with W131 exposed to the solvent.[13] The second conformation of this loop is seen in structures where the cleft is closed, and the loop is tucked in toward the interior of the cleft, burying W131 and allowing van der Waals contacts to exist between residues on either side of the cleft (L128, P129, L132 and I72, I66) (PDB ID 2AGC[11] and PDB ID 1G13[10]). Given that this mobile loop is preceded by an extended disordered chain segment (V122−P129), the mobility of this entire region (V122−T133) can modulate the width of this cleft, and therefore the size of the circumference of the cavity (Figure 1), allowing for lipid ligand to enter into the binding pocket.

The question arises as to whether the features of the protein that are seen in the crystal structure are in conformational exchange in solution and how these various conformations are related to function, as protein mobility and dynamics are often related to function.[22,23] For the case of GM2AP, the multiple conformations in the crystal structure, which in effect modulate the size of the entrance to the cavity, may suggest that a conformational change is necessary for extracting lipid ligand from vesicle surfaces, or that the conformations will be modulated in the halo (lipid bound) or apo protein. Another possible role for the conformational flexibility is in conformational entropy to allow GM2AP to partition with the vesicle surface or to interact with hydrolases, such as HexA, in GM2

dx.doi.org/10.1021/jp505938t | J. Phys. Chem. B 2014, 118, 10607−10617

hydrolysis. To investigate the local structure and mobility of the apolar and mobile loops of GM2AP in solution, we utilized SDSL EPR, which is a powerful spectroscopic tool used to study conformational changes in proteins[24−27] as well as to characterize local backbone motion.[28,29] In addition, MD simulations of GM2AP t conformational sampling were also performed.

EXPERIMENTAL PROCEDURES

Materials. MTSL was purchased from Toronto Research Chemicals, Inc. Unless otherwise stated, all other reagents were from Fisher Scientific and used as received.

Protein Expression, Purification, and Function. Recombinant wild-type GM2AP and cysteine constructs generated for EPR experiments were expressed, purified, and spin labeled as described previously.[13,15,21] Properly folded protein was separated from aggregated and misfolded protein by applying it to an S-200 gel filtration column equilibrated with 50 mM sodium phosphate, 150 mM NaCl, 2.5% glycerol pH 7. Function of each of the labeled constructs, defined as the ability to extract both GM2 and a fluorescently labeled lipid,[15,30] was demonstrated in an earlier study of GM2AP constructs, where power saturation SDSL EPR spectroscopy was used to determine the orientation of this protein on lipid bilayer surfaces.[21] For site L126C, sample homogeneity was further confirmed by mass spectrometry analysis and HPLC analysis, where a single elution peak arose from protein samples collected after SEC and then injected into a C18 column eluted with an acetonitrile and water gradient.[31]

EPR Measurements. Continuous wave X-band EPR spectra for single and double spin labeled GM2AP constructs were collected on a modified Bruker ER-200D spectrometer with an ER023M signal channel, an ER032M field control unit, and a loop gap resonator (Medical Advances, Milwaukee, WI). Spectral scans were collected over the range of 100 Gauss (G) and were recorded with protein samples in sealed round capillaries, 0.60 mm × 0.84 mm × 100 mm (Fiber Optics Center, Inc.; New Bedford, MA), with 3.16 mW incident power and optimized modulation amplitudes. GM2AP spectra were recorded for each of the cysteine variants in solution (50 mM Tris−HCl, pH 7.0). Typical protein concentrations were near 200 μM, and 8−32 scans were collected for each sample. All spectra shown are baseline corrected and integral area normalized using Labview software (Gift from Wayne Hubbell). Pulsed EPR experiment distance measurements for double labeled GM2AP constructs were performed on a Bruker E580 spectrometer with an MD-5 resonator with the four-pulse DEER sequence as described previously.[32−35] DEER data were analyzed with DEERAnalysis2011 software, available online at http://www.epr.ethz.ch/software/index, and in-house Matlab DSim as described previously.[36−38] Because the average distances determined from pulsed experiments for double labeled sites in GM2AP were found to be near 20 Å, low temperature CW EPR experiments were also performed for distance determination.[39−41] Spectra were acquired as 200 G scans at −140 °C with 2 μW incident microwave power. For easy comparison of the degree of line broadening, the spectra are normalized to equal areas and are plotted on the same y-scale. The d_1/d_0 ratio is defined as the height of the high and low field transitions over the height of the center field transition and can be related to distances from measurements of KcsA.[41]

Variable Temperature CW EPR Experiments. For variable temperature CW EPR experiments over the range 5−40 °C, the temperature was controlled by flowing nitrogen gas through a copper coil that was submerged in a refrigerated water bath (Thermo Scientific Neslab RTE-7 Digital One (−25 to 150 ± 0.01 °C)) containing a 40% ethylene glycol (v/v) solution. The cooled nitrogen gas flowed from the copper coil to a quartz Dewar (Wilmad-Labglass, Buena, NJ) that surrounded the loop gap resonator, where the sample was allowed to equilibrate at each temperature for at least 20 min prior to data collection. Temperature was monitored using an Omega microcomputer thermometer model DP703. Temperature stability was ±0.1 °C. For low temperature CW distance measurements, the copper coil was submerged in liquid N_2. The flow rate and length of insulated tubing was optimized to obtain a steady temperature of −140 ± 5 °C.

Line Shape Simulations. MTSL modified cysteine side chains are referred to as R1 labeling. EPR spectra of R1 constructs were simulated using the microscopic order macroscopic disorder (MOMD) model of Freed and colleagues that is freely available at www.acert.cornell.edu.[42] Double integral area normalized EPR spectra were regenerated with either a one- or two-component simulation. Experimental EPR spectra were fit with the MOMD model following the procedure described by Columbus et al. with the following values for the **A** and **g** tensors: A_{xx} = 6, A_{yy} = 6, A_{zz} = 37, g_{xx} = 2.0089, g_{yy} = 2.0021, g_{zz} = 2.0058, and diffusion tilt angles fixed at $\alpha_D = 0°$, $\beta_D = 15°$, and $\gamma_D = 0°$.[28,29] An axially symmetric diffusion tensor was used, with values $R_{||}$ and $R_{\perp}$ where

$$\bar{R} = (R_{||}R_{\perp}^{2})^{1/3} \tag{1}$$

The asymmetry parameter and effective mean correlation time, τ, were calculated using

$$N = R_{||}/R_{\perp} \tag{2}$$

$$\tau = 1/6\bar{R} \tag{3}$$

If a single-component fit did not adequately converge, a two-component model was utilized. In cases where two spectral components were necessary for adequate fitting, to simplify the fitting procedure, the order parameter, C_{20}, for the mobile component was set to 0. The values that were allowed to vary to obtain a least-squares fit were Gib0 (inhomogeneous line width), A_{zz}, $R_{||}$, $R_{\perp}$, and C_{20}.[28]

Determination of Thermodynamic Parameters for Conformational Change of L126R1. The fractional components determined from spectral simulations of the nitroxide line shapes were analyzed in terms of a conformational equilibrium, as has been done previously for other protein systems.[43] The equilibrium expression

$$K_{eq} = f_1/f_2 \tag{4}$$

is defined for the unfolding of the loops, where f_1 is the fraction of the more mobile component and f_2 is the fraction of the less mobile component. Values for the thermodynamic entropy, $\Delta S°$, and enthalpy, $\Delta H°$, of this conformational change were obtained by utilization of the Van't Hoff equation

$$\ln K_{eq} = -\frac{\Delta H°}{RT} + \frac{\Delta S°}{R} \tag{5}$$

NMR HSQC Measurements. Experiments were conducted at 20 °C on a 600 MHz NMR spectrometer equipped with the 1 mM superconducting coil probe (UF-AMRIS). ^{15}N labeled GM2AP was overexpressed in BL21(de3) cells grown in

minimal media supplied with 0.1% ammonium chloride and purified as described previously.[10,15,21] The final sample contains 0.15 mM GM2AP and 20 mM NaOAc at the desired pH. To change the buffer pH, the protein was loaded to a gel filtration column (G25 resin) pre-equilibrated with the desired pH (4.8, 5.6, 6.9) with 20 mM NaOAc. For the GM2 binding experiment, the spectra were collected before and after incubation with a final concentration of 0.6 mM GM2 (in 20 mM NaOAc buffer) at room temperature. The resulting spectra were processed with NMRPipe[44] and Sparky (Goddard and Kneller, Sparky 3, UCSF, San Francisco, CA).

Determination of GM2AP:GM2 Complex Formation. Because little to no conformational change was observed in the EPR/NMR measurements, the formation of the GM2AP:GM2 complex was confirmed for samples where GM2 micelles were added. Specifically, protein:GM2 complexes were purified by size chromatography and the presence of GM2 in the protein fraction was detected via a rescorcinol assay as described previously.[15,30] For both A60R1 and L126R1, differential scanning calorimetry showed an increase in T_m of 0.9 °C of the thermotropic unfolding for the halo protein compared to the unliganded protein, thus further confirming that GM2 was indeed bound to the protein. It is noteworthy that the absolute values of T_m differed for the two constructs, giving an indication of the relative stability of the modified proteins relative to each other (Table S1, Supporting Information).

Molecular Dynamics (MD) Simulations. All MD simulations were performed using the AMBER suite of programs on a potential energy surface described by the *ff99sb*ildn force field.[45,46] Conformers A and C of the crystal structure of the GMA2 protein (PDB ID: 1G13) provided a starting point for our simulations that would help develop an understanding of the conformational ensembles sampled by the protein.[10] Prior to running simulations, charged amino acids were modeled on the basis of their protonation states calculated using the H++ protonation state server.[47] The proteins were solvated in a periodically replicated rectilinear box of explicit SPC/E water molecules,[48] providing an 8 Å solvation layer around the solute molecule. Counterions were added to net-neutralize the solvated system prior to simulations.[49,50] The solvated protein was prepared for production simulations using a well-defined protocol.[51−56] The protein was first energy-minimized over five stages and then equilibrated over two stages using a simulated annealing-like approach. In the first stage of energy minimization, all water molecules and explicit ions were allowed to relax, while all protein atoms were restrained with a strong harmonic potential. In subsequent stages, additional parts of the protein were gradually allowed to relax in solvent. In the second stage of minimization, all hydrogen atoms were allowed to relax. Side chain groups and backbone amide groups followed this in the third and fourth stages, respectively. Finally, in the fifth stage, the entire protein was energy minimized along with the solvent molecules and ions. After energy minimization, the system was slowly heated to 300 K over 100 ps of MD for the canonical ensemble (NVT), while the solute was kept restrained with a weak harmonic potential. In the final stage of equilibration, all restraints were removed from the protein and 1 ns of MD was performed at 300 K for an isothermal and isobaric (NPT) ensemble. After equilibration, MD simulations of both equilibrated systems were propagated for 275 ns in the NPT ensemble at 300 K. A time step of 2 fs was employed, and trajectory information was collected every 1000 steps. A Langevin thermostat[57,58] with a collision frequency of 1 ps^{-1} was employed to maintain the temperature of the system. The SHAKE algorithm[59] was utilized to constrain heavy atom bonds to hydrogen atoms, and long-range electrostatic interactions were calculated using the particle mesh Ewald method.[60] In all, 550 ns of MD data were collected to provide reasonable statistics in understanding the nature of conformational sampling by GMA2P. All analyses were performed using the *ptraj* module of AMBERTools.[46]

RESULTS

Ligand Binding Does Not Alter GM2AP Average Solution Conformation. Ten single CYS variants of GM2AP were generated and labeled with MTSL (referred to within as R1) at the sites shown in Figure 1A. Six of the chosen spin labeled sites are located in the flexible and apolar loops (A60R1, I66R1, I72R1, L126R1, S130R1, and N136R1) and were chosen to investigate the conformational flexibility using EPR spectroscopy. The remaining four CYS variants of GM2AP (V54R1, L87R1, T90R1, and S115R1) were generated to probe sites thought to be either structured (α-helices and β-sheets) or unstructured loop regions of the protein. Figure 2 shows the nitroxide spectra recorded at ambient room temperature for GM2AP in solution under basic pH and acidic pH in the presence of GM2 micelles. The EPR line shapes at each site are consistent with those expected on the basis of the local structure and dynamics reflected in the X-ray structures of GM2AP. This conclusion is draw upon literature reports showing that the R1 line shape correlates with protein structural components and B-factors.[27,61] Of the six sites in the flexible loops and disordered strand regions, A60R1, L126R1, and N136R1 have line shapes consistent with fairly mobile and solvent accessible sites on proteins;[27] however, from the shoulders in these spectra (indicated with arrows), it is clear there are two spectral components (discussed further below). For example, the spectra from site L126R1 are narrow and intense, reflecting a higher degree of motional averaging. This site is located in a flexible strand with very high crystallographic B-factors. Sites I66R1, I72R1, and S130R1 have broadened EPR spectra with structure seen in the high field resonances, which indicate that these spin labeled sites reside in more structured regions of GM2AP. In numerous X-ray structures of GM2AP, the side chains of I66 and I72 can be seen to point in toward the hydrophobic cavity, so it is likely that, at these sites, the spin label motion is restricted by neighboring amino acid side chains as well as the limited space of the cleft leading to the lipid binding pocket. Further, the line shape from site S130R1 is broadened and more reflective of a spin label attached to an alpha helical region of a protein, and some of the crystal structures of GM2AP place this residue in a helical structure.[10,13]

The EPR spectra obtained under acidic conditions in the presence of GM2 micelles are very similar to those obtained under basic pH conditions, suggesting that little to no conformational change has occurred in the presence of ligand. In efforts to further characterize possible conformational changes of the loops upon GM2 ligand binding, two different double CYS constructs were prepared, I66R1/L126R1 and I72R1/S130R1. These sites allow for distance measurements across the loops. The expected experimental values based on conformers in the crystal and MMM (http://www.epr.ethz.ch/software) evaluations of MTSL rotamers range between 16 and 30 Å. Low temperature EPR spectra were collected and

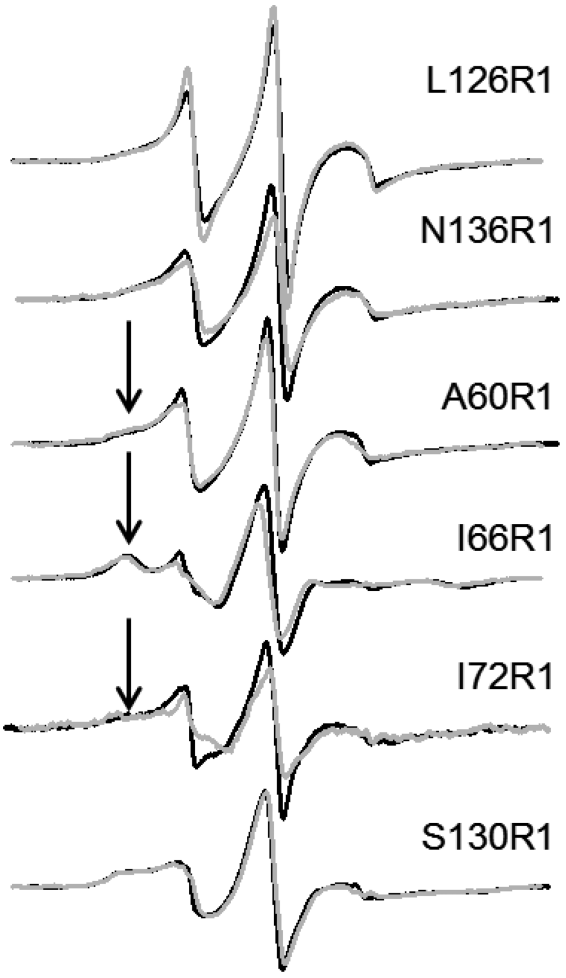

Figure 2. Stack plot of EPR spectra from six sites in the apolar and flexible loops of GM2AP. Spectra were collected at ambient room temperature without temperature regulation. The black traces are for samples prepared in basic pH (8.0), whereas those in gray were collected at pH 4.8 in the presence of 4× molar excess GM2 micelles. All spectra have 100 G sweep widths. Note the spectra obtained for I72R1 in the presence of GM2 showed the most change, but this effect results from protein instability that leads to protein precipitation over time, with increased broadening of the spectral line shape.

analyzed for distances across the binding cleft. As can been seen in the spectra in Figure 3A, very little to no differences were detected in the spectra upon pH change and addition of ligand. The average distances obtained from analysis of the spectral line shapes using the empirical d_1/d_0 parameter[41] are given in Table 1, and values are all between 18 and 20 ± 2 Å. A slight increase of 2 Å in the average distance was seen for I66R1/L126R1 upon addition of GM2 micelles. Because the average distances are near 20 Å, which is the upper limit of distances readily detected by this method,[39,62] pulsed double electron−electron resonance (DEER) spectroscopy[32−34] was also performed for these sites. The background corrected DEER echo curves are shown in Figure 3B. Although MMM modeling of side chain conformers predicted the possibility of larger distances for these sites, DEER data also reported average distances near 20 Å, which is unfortunately a lower distance cutoff for accurate analysis of DEER distance distribution profiles. Nevertheless, the shapes of the echo curves are consistent with an average distance of 20−23 Å, and show that no major conformational changes of these loops occur upon binding GM2 ligand. The lack of distinct oscillations in the DEER echo curve indicates a high degree of conformational flexibility, which is discussed in more detail below.

To further investigate how pH and ligand altered the average conformation of GM2AP, uniformly ^{15}N labeled protein was generated for solution NMR HSQC measurements. Figure 4 shows HSQC spectra of GM2AP at pH 6.9 (purple), pH 5.6 (red), and pH 4.8 (blue) and upon addition of GM2 at pH 4.8 (red = with GM2; blue = absence of GM2). The data show that changes in pH cause a few resonances to shift or disappear, likely as a result of changes in local electrostatic potentials. The binding of GM2 also does not induce shifts in most of the resonances; again, a few peaks are seen to shift or disappear. Assignments for GM2AP are lacking, as the broadening of some peaks indicates intermediate exchange, and we have had low signal intensities in some triple resonance experiments needed for assignments. Future NMR studies are aimed at mapping the specific regions in GM2AP that are altered during pH changes and interactions with ligands; however, these experiments are beyond the scope of this manuscript at this time. Here, the data simply indicate that no major conformational changes occur in GM2AP upon complex formation with GM2 under acidic conditions. The NMR and EPR results are also consistent with CD analyses, which show no detectable changes in the spectra when pH is altered or GM2 micelles are added.

EPR Line Shape Analysis Reveals Conformational Heterogeneity in the Surface Loops of GM2AP. In addition to the above-mentioned six sites in GM2AP, four additional sites were chosen for investigations of conformational heterogeneity. The EPR line shapes of all 10 R1 labeled GM2AP constructs in basic solution with the overlaid simulations are shown in Figure 5. The EPR spectra were simulated using the MOMD model of Freed and colleagues.[42] Using this method, a single component was not sufficient to adequately fit sites in the apolar and flexible loops (A60R1, I66R1, I72R1, L126R1, S130R1, and N136R1). For these sites, we utilized a model where one component was immobile in the intermediate time regimes, whereas the other component had fast-limit mobility where we assumed that this mobile component had $C_{20} = 0$ (the order parameter), as was done previously by others.[28,43] The simulation results are shown in Figure 5. As can be seen in Figure 5A, the two components have dramatically different line shapes, with one having narrow, isotropic-like features, corresponding to a highly mobile site and the other a more broadened line shape corresponding to a site with more restricted motion. Given the presence of two distinct spectra, we can conclude that the conformational exchange is slow on the ns time scale. These two spectral components are reflective of a more mobile and a more immobile spin label environment, consistent with the alternative conformations seen for these flexible regions in the GM2AP X-ray structures.[10−13] The relative percentages of each spectral component are also given in Figure 5A. These alternative spin label conformations may reflect simply spin label conformational states or protein conformational states. These differences are discussed in more detail below.

Variable Temperature SDSL Experiments for Sites L126R1 and I66R1. To further investigate the origin of the multiple-component spectra for sites located in the flexible loop regions of GM2AP, data were collected as a function of temperature over the range 10−35 °C in 5 °C increments. A similar approach has been utilized to characterize a conforma-

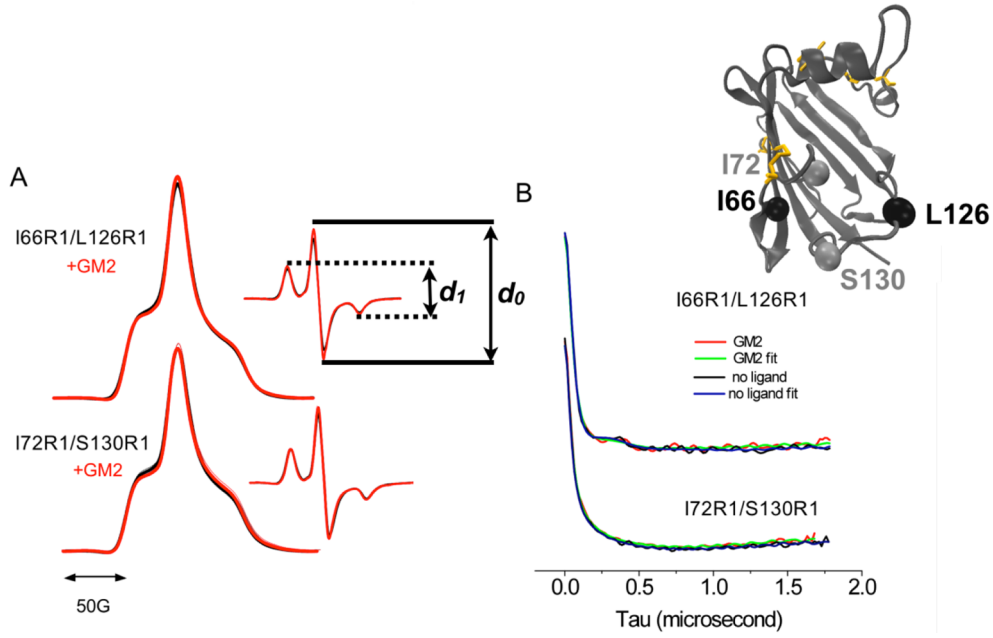

Figure 3. (A) Low temperature integrated absorption and derivative CW EPR spectra of doubly labeled GM2AP constructs I72R1/S130R1 and I66R1/L126R1 showing no change in conformation upon addition of GM2AP. (B) Background corrected DEER echo modulation traces for doubly labeled GM2AP samples showing again no change upon addition of GM2. Distances from both CW and pulsed EPR were estimated to be within the 18−22 Å range and are further discussed within the text.

Table 1. Results of EPR Distance Measurements on GM2AP Constructs without and with GM2

		distance (Å)		
construct	$d_1/d_0 \pm 0.01$	CW ± 2 Å	DEER ± 2 Å	fwhm ± 8 Å
I66R1/L126R1	0.39	18	18	12
I66R1/L126R1 + GM2	0.37	20	18	10
I72R1/S130R1	0.40	18	18	15
I72R1/S130R1 + GM2	0.38	19	18	12

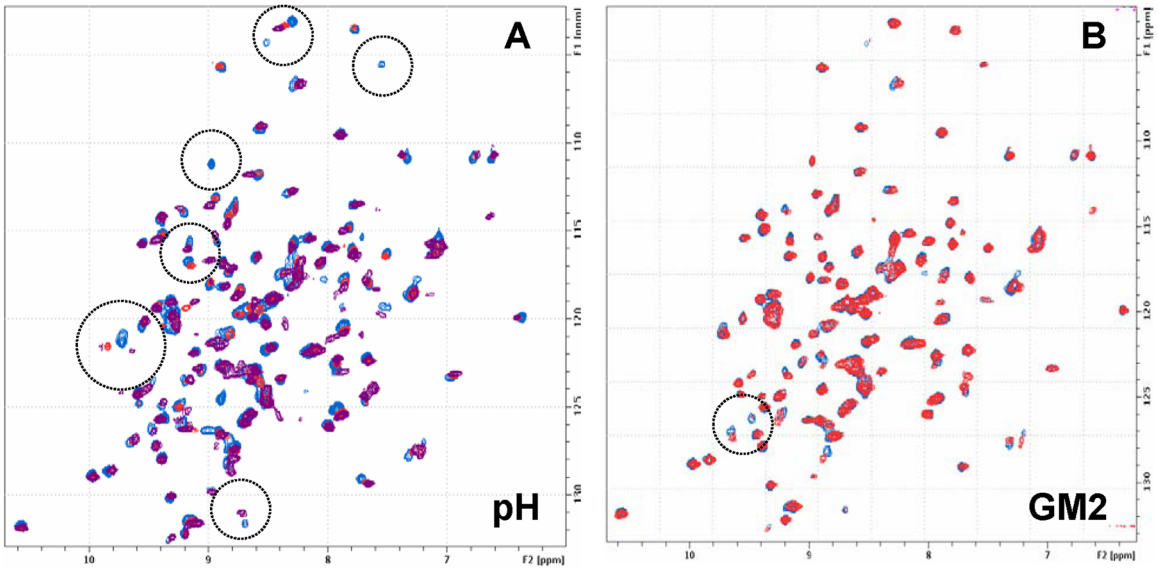

Figure 4. HSQC NMR spectra of uniformly labeled ^{15}N GM2AP (A) at pH 6.8 (purple), pH 5.6 (red), and pH 4.8 (blue) and (B) upon addition of 4× molar excess GM2 micelles (red) at acidic pH 4.8 (blue). Final samples each contain 150 μM GM2AP and 20 mM NaOAc. For the GM2 binding experiments, the spectra were collected before and after incubation with 0.6 mM GM2 at room temperature.

tional change in the transmembrane sequence of the transducer domain of *N. pharaonis* halobacterial transducer of rhodopsins II (NpHtrII) in lipid membranes.[43] For GM2AP, L126R1 in the disordered strand and I66R1 adjacent to the apolar loop were selected for the variable temperature EPR experiments. If these regions of the protein are in conformational exchange, the

dx.doi.org/10.1021/jp505938t | J. Phys. Chem. B 2014, 118, 10607−10617

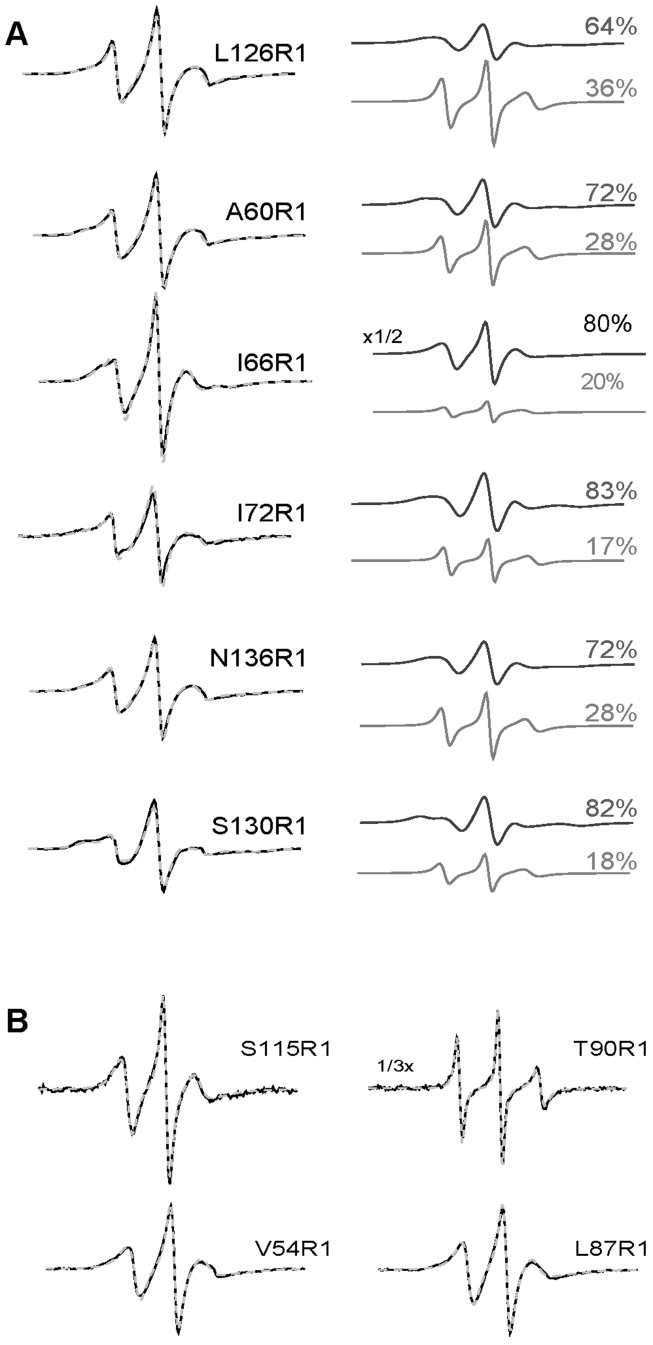

Figure 5. Overlay of area normalized experimental EPR spectra (black) and MOMD simulated spectra (dashed gray) of the 10 spin labeled GM2AP constructs. All spectra have 100 G sweep widths and were collected at ambient room temperature. (A) Spectra for sites that are located in the flexible loops required two components for adequate fitting between the experimental and simulated spectra. These two spectral components are shown, with the more immobile spectrum in black and the mobile spectrum, where C_{20} = 0 was assumed, in gray. (B) Adequate agreement between the experimental and simulated line shapes was obtained for sites V54R1, L87R1, T90R1, and S115R1 (bottom) using only a single spectral component.

equilibrium populations of the two components should change in a linear fashion with inverse temperature. The EPR line shapes obtained at each temperature were then simulated using the MOMD model to extract fractions of populations of the two components. Representative EPR spectra and MOMD simulations of line shapes for L126R1 and I66R1 at select temperatures are shown in Figure 6A. Changes in the EPR line

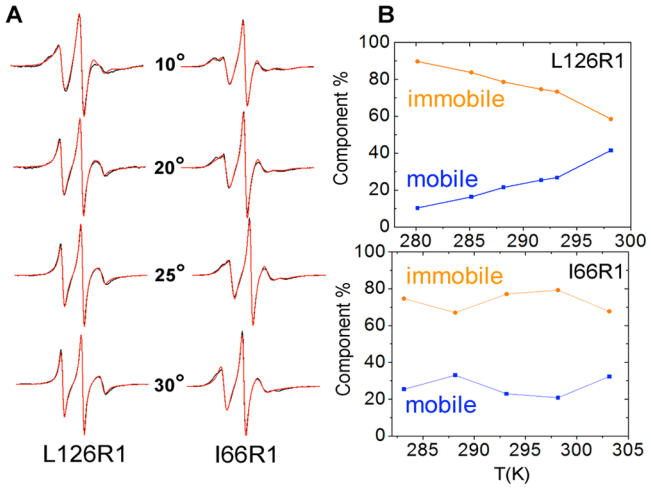

Figure 6. (A) Representative EPR spectra of GM2AP L126R1 and I66R1 as a function of temperature (°C). Overlain experimental spectra (black) and MOMD simulations (red) are shown. Each simulation required two spectral components for an adequate fit to the experimental data. (B) Plots of the relative percentages of the mobile and immobile components obtained from the spectral fits as a function of temperature (K).

shapes were seen for L126R1 with increasing temperature; however, no consistent changes in the I66R1 line shapes were observed. The percentages of the mobile and immobile components were obtained from the line shape fittings for L126R1 and I66R1 and are plotted as a function of temperature (Figure 6B). The plot of component percentages for I66R1 did not show a temperature dependent change, possibly indicating trapped conformers of the spin label and not protein conformational exchange. This interpretation of the data is consistent with the crystal structure, which shows little positional change of the backbone of the segment containing I66 in the three monomers A, B, and C (1G13) and the presence of an ARG-TRP cation pi interaction that may prevent this apolar loop from undergoing marked conformational exchange of the backbone (Figure 1). Therefore, the origin of the two-component spectra at this site may arise from different rotameric states of the spin label.

For L126R1, changes in the EPR line shapes as well as in the relative percentages of the more mobile (f_1) and more immobile (f_2) components were observed as the temperature was varied. Simulations for a select data set can be found in Figure S1 (Supporting Information). At low temperatures, the percent mobile and immobile components were about 10 and 90%, respectively. With increasing temperature, the percentage of the mobile component increased and the percentage of the immobile component decreased until almost equal populations of the two components were seen at ∼30−35 °C. The natural logarithm of the ratio of the fractions of the two components exhibited a linear dependence with inverse temperature (Figure 7). The data shown in Figure 7 were robustly tested for error. The results were collected from two independent experiments performed on two separate samples prepared from different protein expression, refolding, spin labeling, and purification preparations. Finally, different researchers also performed the simulations independently. Results for the relative percentages

dx.doi.org/10.1021/jp505938t | J. Phys. Chem. B 2014, 118, 10607−10617

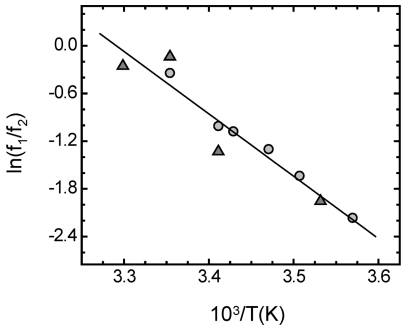

Figure 7. Linear regression of the ratio of the fractions of mobile (f_1) to immobile (f_2) populations plotted for L126R1 as a function of inverse temperature. Two separate EPR data sets were collected from different protein sample preparations, and the simulations were performed independently. The two data sets are indicated by triangles and circles. The solid line is the linear regression from both data sets taken together. From the slope of the line (-7.8 ± 0.8) and the intercept (25.8 ± 2.8), the enthalpy and entropy of loop motion were found to be 65 ± 6 kJ/mol and 215 ± 23 J/(mol K), respectively. The value of the equilibrium constant K at 298.15 K was calculated to be ~0.7.

of each component are strikingly similar. Both data sets and simulations were plotted together, and the slopes of the lines were reproducible within error. The solid line shown is a linear fit of all the data taken together with values of -7.8 ± 0.8 for the slope and 25.8 ± 2.8 for the intercept, from which the enthalpy and entropy of the conformational change were calculated to be 65 ± 6 kJ/mol and 215 ± 23 J/(mol K), respectively. From the values of f_1 and f_2 determined from the spectral fits, the value of the equilibrium constant, K, at 298.15 K was 0.7, indicating that both conformations are easily accessible at physiological temperatures.

L126R1 is located in the conformationally disordered strand of GM2AP.[10] In monomers A and B, the conformation of the loop is such that the side chain of L126 appears to point toward the protein interior, whereas it extends out into the solution in monomer C. The two spectral components determined from fitting with MOMD simulations are consistent with these different environments of the spin label at this site. The immobile component may arise from a fraction of protein conformers having L126R1 pointing in toward the lipid binding cavity, where the motion of the spin label can be restricted by neighboring amino acid side chains as well as by the limited space in the cleft of the cavity entrance. The mobile spectral component is consistent with the strand conformation seen in monomer C, where the spin label would extend out into solution and have a higher degree of rotational freedom.

Conformational Flexibility from Molecular Dynamics Simulations. In an effort to understand the conformational dynamics of the protein, we collected 275 ns of MD data from each of our simulations starting from the distinct conformations observed in monomers A and C of the crystal structure (PDB ID 1G13) of GMA2. We find that both monomers maintained their fold over the course of these simulations while undergoing sizable conformational changes in disordered regions, in good agreement with crystallographic B-factors (Figure S2, Supporting Information). In each simulation, the protein initially sampled conformations similar to its starting point prior to sampling conformational ensembles that were not similar to either starting crystal structure geometry (Figure S3, Supporting Information). Nevertheless, further analyses reveal that there is considerable overlap (Figure S3, Supporting Information) among the calculated population distributions of root-mean-square deviation (RMSD) values calculated for protein backbone atoms over both simulations, and a combined trajectory with respect to the crystal structure conformation of monomer A, suggesting both simulations sample similar conformational space.

The beta-sheet regions of GM2AP arrange to form a hydrophobic cavity that changes over the course of our simulations. As such, the volume of the cavity described by the protein backbone provides a useful metric that describes the conformational changes of GM2AP, which avoids alignment issues common in RMSD calculations. Toward this end, we analyzed the volume of the protein cavity using the recently developed trj_cavity utility that helps identify and quantitatively characterize cavities observed over the course of a MD simulation (Figure S4, Supporting Information).[63] Default program parameters were employed for the grid and nearest neighbor search for a four-sided cavity. Our analysis of cavity volumes finds that GM2AP once again samples similar conformational ensembles in both simulations. We find that, although the cavity volume differed in the two crystal structure conformations of the protein, there was much similarity in the volumes sampled by the protein in our calculations (Figure S4, Supporting Information). In close agreement with our EPR data and RMSD data, these volume analyses further indicate that crystal-packing effects likely influenced the distinct protein conformations observed in the crystal structure. This is not all together surprising, as crystal packing effects have been known to influence the protein structures, such as in the case of the paradigm zinc-sensor protein CzrA.[53,54,56] Taken together, these results indicate that the monomer conformations observed in the crystal structures of GM2AP likely represent trapped states. Although the GM2AP structure would sample these higher-energy conformations from time to time, it would predominantly sample an ensemble of conformations having the characteristics of both conformers in solution.

We next investigated the mobility of protein residues from our MD simulations to build an understanding of the role of residue mobility and the associated changes in protein structure in GM2AP function. Toward this end, we calculated the root-mean-square fluctuations (RMSFs) for backbone Cα carbon atoms of each residue for structures obtained from both simulations (Figure 8). Our calculations revealed a number of mobile and immobile regions in the protein. In particular, we find that regions predicted in GM2AP to have high mobility or disorder from crystallographic B-factors (Figure S2, Supporting Information) were also highly mobile in both simulations, allowing it to sample multiple conformations. In favorable agreement with EPR data, results show that A60, I66, I72, L126, and S130 residues and their neighboring residues are mobile in these simulations (Figure 8).

To better characterize the conformational sampling at these sites, we performed a clustering analysis on the protein conformations sampled over the course of the simulations. In this calculation, all protein conformations from MD simulations were first aligned against the crystal structure conformation of monomer A. The implementation of the "average linkage" clustering algorithm in AMBERTools was then used to cluster L126, A60, I66, I72, N136, and S130 residues individually.[46] In favorable agreement with the EPR data, our calculations suggest that these residues likely exist in distinct major and minor conformational states (Figure 9).

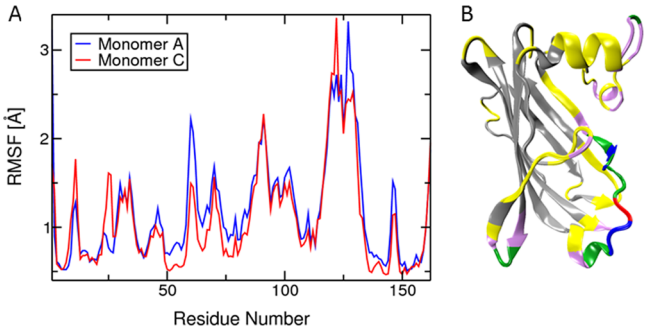

Figure 8. (A) Root mean square fluctuation (RMSF) profiles of MD trajectories from simulations of monomer A and monomer B. These values were calculated for protein backbone Cα carbon atoms for each residue. (B) Ribbon diagram of monomer A where the color coding represents the range of RMSF values as follows: The color code used is gray (0.0–1.0 Å), yellow (1.0–1.5 Å), purple (1.5–2.0 Å), blue (2.0–2.5 Å), green (2.5–3.0 Å), and red (3.0–4.0 Å).

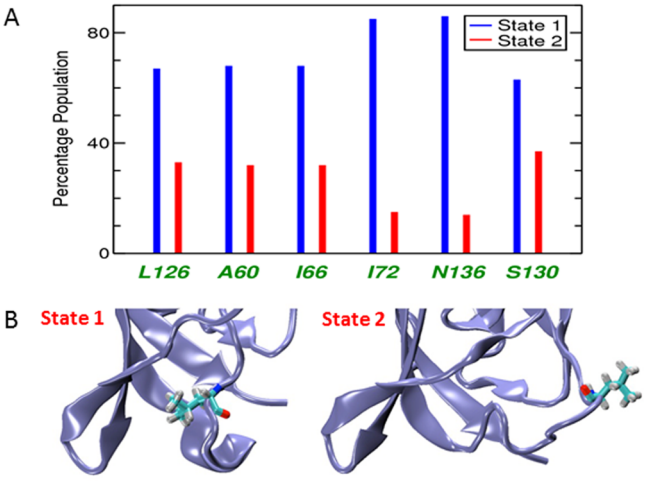

Figure 9. (A) Percentage of protein structures observed bearing distinct conformations of L126, A60, I66, I72, N136, and S130 residues over 550 ns of MD data. These percentage populations were calculated for all conformations sampled in our simulations starting from the crystal structures of monomers A and C. All snapshots of protein structures were first aligned to the crystal structure of monomer A based on their backbone atoms. A clustering analysis for each residue followed this step. (B) Ribbon diagrams showing the positions of the L126 side chain in representative structures obtained from the clustering analysis. In state 1, the side chains point toward the protein interior, whereas, in state 2, the side chains were seen to point out toward the solvent.

Figure 9B shows representative structures for the L126 side chain from this clustering process. Remarkably, the orientations of the side chains are reflective of the two states observed in the crystal structures of monomers A and C, where one side chain points in toward the protein interior and the other is more solvent exposed and likely more mobile. For I66, a similar trend is also observed: one is buried with close contact to W131, whereas the other state is not interacting with W131. For sites I72 and N136, the two clustered states also differed in that one state is more buried and the other more solvent exposed. For S130, the states differed in the degree of H-bonding that the serine participated in with a neighboring loop. For A60, however, the methyl side chain remains solvent exposed in both clusters and no significant differences in side chain packing are observed. The states reported from the clustering analysis for A60 represent different orientations of this extended apolar loop. These conformations likely result from promiscuity/heterogeneity in E58 side chain interactions to either form a hydrogen bond with N136 or a weak anion–π interaction with the aromatic ring of W63. Clustering analysis of the EPR control sites V54, T90, S115, and L87 reveals only a single cluster for T90 and V54. Two states with populations of 85/15 (%/%) for both L87 and S115 are observed. As can be seen in Figure 8, both of these sites reside in well-defined secondary structural elements (L87 in an α-helix and S115 in a β-strand). MD results, however, show these elements to have moderate mobility (color coded yellow in Figure 8). The clustering results for these two sites reflect different positions of the helix/strand with no variation in the side chain rotamers. Taken together, our calculations support the results obtained from EPR investigations, showing that conformational exchange exists in solution and that the X-ray structures likely represent this solution conformational heterogeneity.

CONCLUSIONS

SDSL was utilized to investigate the flexible loop regions of GM2AP. GM2AP has eight native cysteines that form four disulfide bonds essential for the stability of exposed loop regions. We were able to engineer additional cysteines at various sites and express, purify, and isolate homogeneous samples of spin labeled GM2AP. Analysis of the EPR spectral line shapes and MOMD simulations for spin labels in the disordered chain segment and both loops are consistent with the various conformations seen in X-ray structures. Multiple conformations of the mobile loop *in solution* were detected by EPR and MD simulations, indicating that the conformations seen in the crystal structure are present in solution and may play a functional role in ligand binding or interactions with lipid vesicles. SDSL and NMR HSQC titrations show minimal structural perturbations upon addition of GM2 ligand or with changes in pH. Future work is focused on assessing the role loop flexibility plays in GM2AP function.

ASSOCIATED CONTENT

Supporting Information

Protein sample preparation, spin labeling approach, control experimental data, NMR data, and further results from MD simulations are described. This material is available free of charge via the Internet at http://pubs.acs.org.

AUTHOR INFORMATION

Corresponding Author

*Phone: +1 352 392 2345. Fax: +1 352 392 0872. E-mail: fanucci@chem.ufl.edu.

Present Addresses

[⊥](J.D.C.) 3012 Seville St, Fort Lauderdale, FL 33304, USA.
[#](J.D.M.) One Diamond Causeway Suite 21/352, Savannah, GA 31406, USA.
[○](Y.R.) Department of Neuroscience College of Medicine, Center for Translational Research in Neurodegenerative Disease, University of Florida, Gainesville, FL 32610, USA.
[▽](L.G.) Syngenta Crop Protection, Inc., 410 S Swing Rd, Greensboro, NC 27409, USA.
[&](P.W.D'A.) Herbert Wertheim College of Medicine, 11200 SW Eighth Street, AHC2, Miami, FL 3319, USA.

Notes

The authors declare no competing financial interest.

■ ACKNOWLEDGMENTS

This work was supported by NIH grants GM077232 (G.E.F.) and GM60603 (C.S.W) and NSF-EPSCoR Louisiana Alliance for Simulation-Guided Materials Applications EPS-1003897 (D.K.C.), the Louisiana Board of Regents LEQSF-EPS(2014)-PFUND-388 (D.K.C.), and the State of Florida (G.E.F.). We are grateful to the Center of Structural Biology at UF for use of the circular dichroism spectrometer, to Jim Rocca and the Users Program of the National High Magnetic Field Laboratory and Advanced Magnetic Resonance Imaging and Spectroscopy Facility (AMRIS) of the University of Florida for access to NMR instrumentation and assistance with collecting the NMR data, to Kieu-Trang Tran for assisting in collecting MD data, and to Christian Altenbach and Wayne Hubbell for kindly supplying Labview software.

■ ABBREVIATIONS

SAP, sphingolipid activator protein; GM2AP, GM2 activator protein; HexA, hexosaminidase A; MTSL, (1-oxyl-2,2,5,5-tetramethyl-Δ3-pyrroline-3-methyl) methanethiosulfonate spin label; GM2, GM2 ganglioside; SDSL, site-directed spin labeling; EPR, electron paramagnetic resonance; NMR, nuclear magnetic resonance; CD, circular dichroism; CD1, cluster of differentiation 1; MS, mass spectrometry; MD, molecular dynamics; NaOAc, sodium acetate; RMSD, root-mean-square deviation; RMSF, root-mean-square fluctuations

■ REFERENCES

(1) Kolter, T.; Sandhoff, K. Principles of Lysosomal Membrane Digestion: Stimulation of Sphingolipid Degradation by Sphingolipid Activator Proteins and Anionic Lysosomal Lipids. *Annu. Rev. Cell Dev. Biol.* **2005**, *21*, 81−103.

(2) Schulze, H.; Kolter, T.; Sandhoff, K. Principles of Lysosomal Membrane Degradation: Cellular Topology and Biochemistry of Lysosomal Lipid Degradation. *Biochim. Biophys. Acta* **2009**, *1793*, 674−683.

(3) Sandhoff, K.; Kolter, T. Glycolipids of the Cell Surface−Biochemistry of Their Decomposition. *Naturwissenschaften* **1995**, *82*, 403−413.

(4) Griffiths, G.; Hoflack, B.; Simons, K.; Mellman, I.; Kornfeld, S. The Mannose 6-Phosphate Receptor and the Biogenesis of Lysosomes. *Cell* **1988**, *52*, 329−341.

(5) Sandhoff, K.; Kolter, T. Topology of Glycosphingolipid Degradation. *Trends. Cell Biol.* **1996**, *6*, 98−103.

(6) Mahuran, D. J. The Gm2 Activator Protein, Its Roles as a Co-Factor in Gm2 Hydrolysis and as a General Glycolipid Transport Protein. *Biochim. Biophys. Acta* **1998**, *1393*, 1−18.

(7) Schroder, M.; Schnabel, D.; Suzuki, K.; Sandhoff, K. A Mutation in the Gene of a Glycolipid-Binding Protein (Gm2 Activator) That Causes Gm2-Gangliosidosis Variant AB. *FEBS Lett.* **1991**, *290*, 1−3.

(8) Gravel, R.; Clarke, J.; Kaback, M.; Mahuran, D.; Sandhoff, K.; Suzuki, K. *The Gm2 Gangliosidoses*, 7th ed.; McGraw-Hill Inc.: New York, 1995.

(9) Wright, C. S.; Li, S. C. Crystallization and Preliminary X-Ray Characterization of Gm2-Activator Protein. *Acta Crystallogr., Sect. D: Biol. Crystallogr.* **1997**, *53*, 211−212.

(10) Wright, C. S.; Li, S. C.; Rastinejad, F. Crystal Structure of Human Gm2-Activator Protein with a Novel Beta-Cup Topology. *J. Mol. Biol.* **2000**, *304*, 411−422.

(11) Wright, C. S.; Mi, L. Z.; Lee, S.; Rastinejad, F. Crystal Structure Analysis of Phosphatidylcholine-Gm2-Activator Product Complexes: Evidence for Hydrolase Activity. *Biochemistry* **2005**, *44*, 13510−13521.

(12) Wright, C. S.; Mi, L. Z.; Rastinejad, F. Evidence for Lipid Packaging in the Crystal Structure of the Gm2-Activator Complex with Platelet Activating Factor. *J. Mol. Biol.* **2004**, *342*, 585−592.

(13) Wright, C. S.; Zhao, Q.; Rastinejad, F. Structural Analysis of Lipid Complexes of Gm2-Activator Protein. *J. Mol. Biol.* **2003**, *331*, 951−964.

(14) Conzelmann, E.; Burg, J.; Stephan, G.; Sandhoff, K. Complexing of Glycolipids and Their Transfer between Membranes by the Activator Protein for Degradation of Lysosomal Ganglioside Gm2. *Eur. J. Biochem.* **1982**, *123*, 455−464.

(15) Ran, Y.; Fanucci, G. E. Ligand Extraction Properties of the Gm2 Activator Protein and Its Interactions with Lipid Vesicles. *Biophys. J.* **2009**, *97*, 257−266.

(16) Rigat, B.; Wang, W.; Leung, A.; Mahuran, D. J. Two Mechanisms for the Recapture of Extracellular Gm2 Activator Protein: Evidence for a Major Secretory Form of the Protein. *Biochemistry* **1997**, *36*, 8325−8331.

(17) Rigat, B.; Yeger, H.; Shehnaz, D.; Mahuran, D. Gm2 Activator Protein Inhibits Platelet Activating Factor Signaling in Rats. *Biochem. Biophys. Res. Commun.* **2009**, *385*, 576−580.

(18) Major, A. S.; Joyce, S.; Van Kaer, L. Lipid Metabolism, Atherogenesis and Cd1-Restricted Antigen Presentation. *Trends Mol. Med.* **2006**, *12*, 270−278.

(19) Zhou, D.; Cantu, C., 3rd; Sagiv, Y.; Schrantz, N.; Kulkarni, A. B.; Qi, X.; Mahuran, D. J.; Morales, C. R.; Grabowski, G. A.; Benlagha, K.; et al. Editing of Cd1d-Bound Lipid Antigens by Endosomal Lipid Transfer Proteins. *Science* **2004**, *303*, 523−527.

(20) Giehl, A.; Lemm, T.; Bartelsen, O.; Sandhoff, K.; Blume, A. Interaction of the GM2-Activator Protein with Phospholipid-Ganglioside Bilayer Membranes and with Monolayers at the Air-Water Interface. *Eur. J. Biochem.* **1999**, *261*, 650−658.

(21) Mathias, J. D.; Ran, Y.; Carter, J. D.; Fanucci, G. E. Interactions of the GM2 Activator Protein with Phosphatidylcholine Bilayers: A Site Directed Spin Labeling Power Saturation Study. *Biophys. J.* **2009**, *97*, 1436−1444.

(22) Clore, G. M. Visualizing Lowly-Populated Regions of the Free Energy Landscape of Macromolecular Complexes by Paramagnetic Relaxation Enhancement. *Mol. Biosyst.* **2008**, *4*, 1058−1069.

(23) Smock, R. G.; Gierasch, L. M. Sending Signals Dynamically. *Science* **2009**, *324*, 198−203.

(24) Fanucci, G. E.; Cadieux, N.; Piedmont, C. A.; Kadner, R. J.; Cafiso, D. S. Structure and Dynamics of the Beta-Barrel of the Membrane Transporter Btub by Site-Directed Spin Labeling. *Biochemistry* **2002**, *41*, 11543−11551.

(25) Fanucci, G. E.; Cafiso, D. S. Recent Advances and Applications of Site-Directed Spin Labeling. *Curr. Opin. Struct. Biol.* **2006**, *16*, 644−653.

(26) Hubbell, W. L.; Cafiso, D. S.; Altenbach, C. Identifying Conformational Changes with Site-Directed Spin Labeling. *Nat. Struct. Biol.* **2000**, *7*, 735−739.

(27) McHaourab, H. S.; Lietzow, M. A.; Hideg, K.; Hubbell, W. L. Motion of Spin-Labeled Side Chains in T4 Lysozyme. Correlation with Protein Structure and Dynamics. *Biochemistry* **1996**, *35*, 7692−7704.

(28) Columbus, L.; Hubbell, W. L. Mapping Backbone Dynamics in Solution with Site-Directed Spin Labeling: Gcn4−58 Bzip Free and Bound to DNA. *Biochemistry* **2004**, *43*, 7273−7287.

(29) Columbus, L.; Kalai, T.; Jeko, J.; Hideg, K.; Hubbell, W. L. Molecular Motion of Spin Labeled Side Chains in Alpha-Helices: Analysis by Variation of Side Chain Structure. *Biochemistry* **2001**, *40*, 3828−3846.

(30) Ran, Y.; Fanucci, G. E. A Dansyl Fluorescence-Based Assay for Monitoring Kinetics of Lipid Extraction and Transfer. *Anal. Biochem.* **2008**, *382*, 132−134.

(31) Tipton, J. D.; Carter, J. D.; Mathias, J. D.; Emmett, M. R.; Fanucci, G. E.; Marshall, A. G. Sequential Proteolysis and High-Field Fticr Ms to Determine Disulfide Connectivity and 4-Maleimide Tempo Spin-Label Location in L126c Gm2 Activator Protein. *Anal. Chem.* **2009**, *81*, 7611−7617.

(32) Jeschke, G. Deer Distance Measurements on Proteins. *Annu. Rev. Phys. Chem.* **2012**, *63*, 419−446.
(33) Jeschke, G.; Polyhach, Y. Distance Measurements on Spin-Labelled Biomacromolecules by Pulsed Electron Paramagnetic Resonance. *Phys. Chem. Chem. Phys.* **2007**, *9*, 1895−1910.
(34) Pannier, M.; Veit, S.; Godt, A.; Jeschke, G.; Spiess, H. W. Dead-Time Free Measurement of Dipole-Dipole Interactions between Electron Spins. *J. Magn. Reson.* **2000**, *142*, 331−340.
(35) Galiano, L.; Bonora, M.; Fanucci, G. E. Interflap Distances in Hiv-1 Protease Determined by Pulsed Epr Measurements. *J. Am. Chem. Soc.* **2007**, *129*, 11004−11005.
(36) Blackburn, M. E.; Veloro, A. M.; Fanucci, G. E. Monitoring Inhibitor-Induced Conformational Population Shifts in Hiv-1 Protease by Pulsed Epr Spectroscopy. *Biochemistry* **2009**, *48*, 8765−8767.
(37) Kear, J. L.; Blackburn, M. E.; Veloro, A. M.; Dunn, B. M.; Fanucci, G. E. Subtype Polymorphisms among Hiv-1 Protease Variants Confer Altered Flap Conformations and Flexibility. *J. Am. Chem. Soc.* **2009**, *131*, 14650−14651.
(38) Huang, X.; Britto, M. D.; Kear, J. L.; Christopher, B. D.; Rocca, J. R.; Simmerling, C.; McKenna, R.; Bieri, M.; Gooley, P. R.; Dunn, B. M.; et al. The Role of Select Subtype Polymorphisms on Hiv-1 Protease Conformational Sampling and Dynamics. *J. Biol. Chem.* **2014**, *289*, 17203−17214.
(39) Altenbach, C.; Oh, K. J.; Trabanino, R. J.; Hideg, K.; Hubbell, W. L. Estimation of Inter-Residue Distances in Spin Labeled Proteins at Physiological Temperatures: Experimental Strategies and Practical Limitations. *Biochemistry* **2001**, *40*, 15471−15482.
(40) Fanucci, G. E.; Coggshall, K. A.; Cadieux, N.; Kim, M.; Kadner, R. J.; Cafiso, D. S. Substrate-Induced Conformational Changes of the Periplasmic N-Terminus of an Outer-Membrane Transporter by Site-Directed Spin Labeling. *Biochemistry* **2003**, *42*, 1391−1400.
(41) Gross, A.; Columbus, L.; Hideg, K.; Altenbach, C.; Hubbell, W. L. Structure of the Kcsa Potassium Channel from Streptomyces Lividans: A Site-Directed Spin Labeling Study of the Second Transmembrane Segment. *Biochemistry* **1999**, *38*, 10324−10335.
(42) Budil, D. E.; Lee, S.; Saxena, S.; Freed, J. H. Nonlinear-Least-Squares Analysis of Slow-Motion Epr Spectra in One and Two Dimensions Using a Modified Levenberg-Marquardt Algorithm. *J. Magn. Reson.* **1996**, *120*, 155−189.
(43) Bordignon, E.; Klare, J. P.; Doebber, M.; Wegener, A. A.; Martell, S.; Engelhard, M.; Steinhoff, H. J. Structural Analysis of a Hamp Domain: The Linker Region of the Phototransducer in Complex with Sensory Rhodopsin Ii. *J. Biol. Chem.* **2005**, *280*, 38767−38775.
(44) Delaglio, F.; Grzesiek, S.; Vuister, G. W.; Zhu, G.; Pfeifer, J.; Bax, A. Nmrpipe - a Multidimensional Spectral Processing System Based on Unix Pipes. *J. Biomol. NMR* **1995**, *6*, 277−293.
(45) Lindorff-Larsen, K.; Piana, S.; Palmo, K.; Maragakis, P.; Klepeis, J. L.; Dror, R. O.; Shaw, D. E. Improved Side-Chain Torsion Potentials for the Amber Ff99sb Protein Force Field. *Proteins* **2010**, *78*, 1950−1958.
(46) Case, D. A.; Cheatham, T. E., III; Darden, T.; Gohlke, H.; Luo, R.; Merz, K. M., Jr.; Onufriev, A.; Simmerling, C.; Wang, B.; Woods, R. The Amber Biomolecular Simulation Programs. *J. Comput. Chem.* **2005**, *26*, 1668−1688.
(47) Gordon, J. C.; Myers, J. B.; Folta, T.; Shoja, V.; Heath, L. S.; Onufriev, A. H++: A Server for Estimating Pkas and Adding Missing Hydrogens to Macromolecules. *Nucleic Acids Res.* **2005**, *33*, W368−371.
(48) Jorgensen, W. L.; Chandrasekhar, J.; Madura, J. D.; Impey, R. W.; Klein, M. L. Comparison of Simple Potential Functions for Simulating Liquid Water. *J. Chem. Phys.* **1983**, *79*, 926−935.
(49) Li, P. F.; Roberts, B. P.; Chakravorty, D. K.; Merz, K. M. Rational Design of Particle Mesh Ewald Compatible Lennard-Jones Parameters for +2 Metal Cations in Explicit Solvent. *J. Chem. Theory Comput.* **2013**, *9*, 2733−2748.
(50) Joung, I. S.; Cheatham, T. E. Determination of Alkali and Halide Monovalent Ion Parameters for Use in Explicitly Solvated Biomolecular Simulations. *J. Phys. Chem. B* **2008**, *112*, 9020−9041.
(51) Lee, C. W.; Chakravorty, D. K.; Chang, F. M. J.; Reyes-Caballero, H.; Ye, Y. Z.; Merz, K. M.; Giedroc, D. P. Solution Structure of Mycobacterium Tuberculosis Nmtr in the Apo State: Insights into Ni(Ii)-Mediated Allostery. *Biochemistry* **2012**, *51*, 2619−2629.
(52) Chakravorty, D. K.; Wang, B.; Ucisik, M. N.; Merz, K. M. Insight into the Cation-Pi Interaction at the Metal Binding Site of the Copper Metallochaperone Cusf. *J. Am. Chem. Soc.* **2011**, *133*, 19330−19333.
(53) Chakravorty, D. K.; Wang, B.; Lee, C. W.; Giedroc, D. P.; Merz, K. M. Simulations of Allosteric Motions in the Zinc Sensor Czra. *J. Am. Chem. Soc.* **2012**, *134*, 3367−3376.
(54) Chakravorty, D. K.; Parker, T. M.; Guerra, A. J.; Sherrill, C. D.; Giedroc, D. P.; Merz, K. M. Energetics of Zinc-Mediated Interactions in the Allosteric Pathways of Metal Sensor Proteins. *J. Am. Chem. Soc.* **2013**, *135*, 30−33.
(55) Chakravorty, D. K.; Hammes-Schiffer, S. Impact of Mutation on Proton Transfer Reactions in Ketosteroid Isomerase: Insights from Molecular Dynamics Simulations. *J. Am. Chem. Soc.* **2010**, *132*, 7549−7555.
(56) Chakravorty, D. K.; Wang, B.; Lee, C. W.; Guerra, A. J.; Giedroc, D. P.; Merz, K. M. Solution Nmr Refinement of a Metal Ion Bound Protein Using Metal Ion Inclusive Restrained Molecular Dynamics Methods. *J. Biomol. NMR* **2013**, *56*, 125−137.
(57) Doll, J. D.; Dion, D. R. Generalized Langevin Equation Approach for Atom-Solid-Surface Scattering - Numerical Techniques for Gaussian Generalized Langevin Dynamics. *J. Chem. Phys.* **1976**, *65*, 3762−3766.
(58) Adelman, S. A.; Doll, J. D. Generalized Langevin Equation Approach for Atom-Solid-Surface Scattering - General Formulation for Classical Scattering Off Harmonic Solids. *J. Chem. Phys.* **1976**, *64*, 2375−2388.
(59) Allen, M. P.; Tildesley, D. J. *Computer Simulations of Liquids*; Clarenden Press: Oxford, U.K., 1987.
(60) York, D. M.; Darden, T. A.; Pedersen, L. G. The Effect of Long-Range Electrostatic Interactions in Simulations of Macromolecular Crystals - a Comparison of the Ewald and Truncated List Methods. *J. Chem. Phys.* **1993**, *99*, 8345−8348.
(61) Xu, Q.; Kim, M.; Ho, K. W.; Lachowicz, P.; Fanucci, G. E.; Cafiso, D. S. Membrane Hydrocarbon Thickness Modulates the Dynamics of a Membrane Transport Protein. *Biophys. J.* **2008**, *95*, 2849−2858.
(62) Rabenstein, M. D.; Shin, Y. K. Determination of the Distance between Two Spin Labels Attached to a Macromolecule. *Proc. Natl. Acad. Sci. U. S. A.* **1995**, *92*, 8239−8243.
(63) Paramo, T.; East, A.; Garzon, D.; Ulmschneider, M. B.; Bond, P. J. Efficient Characterization of Protein Cavities within Molecular Simulation Trajectories: Trj_Cavity. *J. Chem. Theory Comput.* **2014**, *10*, 2151−2164.